nature nanotechnology

LETTERS

PUBLISHED ONLINE: 23 DECEMBER 2012 | DOI: 10.1038/NNANO.2012.217

Growth of a two-dimensional dielectric monolayer on quasi-freestanding graphene

Rafik Addou, Arjun Dahal and Matthias Batzill*

Integrating graphene into device architectures requires interfacing graphene with dielectric materials[1–3]. However, the dewetting and thermal instability of dielectric layers on top of graphene makes fabricating continuous graphene/dielectric interfaces challenging[4–9]. Here, we show that yttria (Y_2O_3)—a high-κ dielectric—can form a complete monolayer on platinum-supported graphene. The monolayer interacts weakly with graphene, but is stable to high temperatures. Scanning tunnelling microscopy reveals that the yttria layer exhibits a two-dimensional hexagonal lattice rotated by 30° relative to the hexagonal graphene lattice. X-ray photoemission spectroscopy measurements indicate a shift of the Fermi level in graphene on yttria deposition, which suggests that dielectric layers could be used for charge doping of metal-supported graphene.

Previous fundamental studies have focused on stacking exfoliated graphene on dielectric substrates[10–13]. The exfoliation of other two-dimensional van der Waals materials[14] has the potential to allow different materials to be arbitrarily stacked with the graphene. The interaction between graphene and these other two-dimensional materials is weak and therefore only minimally affects the electronic properties of the graphene. However, although mechanical stacking of exfoliated molecular layers results in unique materials for basic research and device demonstration[15], the lack of scalability makes this approach unlikely to be of use in device fabrication.

The growth of artificial heterostructures using molecular beam epitaxy (MBE) or chemical vapour deposition (CVD) would provide the necessary scalability. However, growing high-quality dielectric materials directly on graphene is problematic. In particular, graphene has a low surface energy, so most materials do not wet graphene, which leads to three-dimensional growth. To address this issue, graphene has been chemically modified[4] (for example, by fluorine[5], ozone[6], and organic[7] or inorganic[8,9] nucleation layers) before the growth of metal-oxide dielectric materials. However, yttria (Y_2O_3) has recently demonstrated favourable wetting behaviour on graphene and carbon nanotubes, and could therefore be a promising dielectric material for the creation of graphene devices[16,17].

Here, we characterize the initial growth (monolayer regime) of yttria on graphene. As a substrate we chose graphene supported on a Pt(111) single-crystal surface. It is well known that graphene interacts weakly with a platinum surface[18,19], so platinum-supported graphene behaves (except for a small p-type doping effect due to the large workfunction of platinum[20]) like free-standing graphene[21]. Graphene on platinum therefore has very similar properties to graphene supported on copper, iridium or other late transition metals[18]. Furthermore, synthesis over metal films is one of the most promising approaches for large-scale graphene synthesis[22,23], so the direct growth of dielectric layers on metal-supported graphene may be incorporated into large-scale graphene/dielectric heterostructure synthesis. However, in contrast to when using copper, monolayer graphene can be synthesized easily in ultrahigh vacuum (UHV) on platinum, making platinum a preferred material for fundamental surface science investigations of graphene.

Here, monolayer graphene has been grown in UHV by exposure of a clean Pt(111) single crystal to 1×10^{-7} torr ethene, with the sample at 700 °C. This leads to the formation of several rotational domains of monolayer graphene, as demonstrated by low-energy electron diffraction (LEED) and scanning tunnelling microscopy (STM) (Supplementary Fig. S1). Because of the lattice mismatch between graphene and platinum, and depending on the rotational alignment between graphene and the Pt(111) substrate, different moiré superstructures are observed[19,24,25].

Yttria was grown on top of the graphene/Pt(111) substrate at room temperature by reactive vapour deposition of yttrium in a 1×10^{-7} torr O_2 atmosphere. Even with deposition at room temperature, for the monolayer regime the yttria covers the surface uniformly in a two-dimensional layer (Supplementary Fig. S2). However, ordered structures only appear after annealing to above 550 °C. In the following, the ordered yttria-covered samples obtained after annealing up to 700 °C were characterized *in situ* by LEED, STM, X-ray photoemission spectroscopy (XPS) and Auger electron spectroscopy (AES).

In LEED we only observe the diffraction pattern of the graphene/Pt(111) system (Supplementary Fig. S1). Owing to the many different rotational domains of graphene, the diffraction from the graphene appears as an (interrupted) circle with a radius corresponding to the inverse graphene lattice constant. Even with a complete monolayer of yttria on graphene we only observe the graphene rings, indicating that the graphene remains intact and the yttria diffraction is too weak to be detected in our experimental setup. In contrast, the growth of monolayer amounts of yttria in the absence of graphene, that is, on pure Pt(111), results in a well-defined coincidence structure relative to the Pt(111) substrate with a large unit cell of $(5\sqrt{3} \times 2\sqrt{3})$ R30°, with a clearly defined LEED diffraction pattern and well-ordered monolayer structures in STM (Supplementary Fig. S3). This difference between yttria growth on graphene/Pt(111) and on pure Pt(111) illustrates that the yttria film remains on top of the graphene and does not directly interact with the Pt(111) surface.

Further verification of the growth of an yttria/graphene/Pt(111) sandwich structure was drawn from AES measurements, which indicate identical attenuation of the carbon and platinum AES signal by the yttria film (Supplementary Fig. S4), a clear indication of a layered structure with the oxide growing on top of the graphene/Pt(111) substrate. Importantly, the AES carbon peak shape, shown in Fig. 1a,b, retains the characteristic line shape for sp^2 carbon[26] throughout the experiments up to annealing temperatures of 750 °C, when carbon dissolves into the platinum bulk. This is confirmation that the graphene sheet is undisturbed throughout our experiments, thus demonstrating the high thermal stability of the yttria/graphene/Pt(111) sandwich structure.

Department of Physics, University of South Florida, Tampa, Florida 33620, USA. *e-mail: mbatzill@usf.edu

© 2013 Macmillan Publishers Limited. All rights reserved.

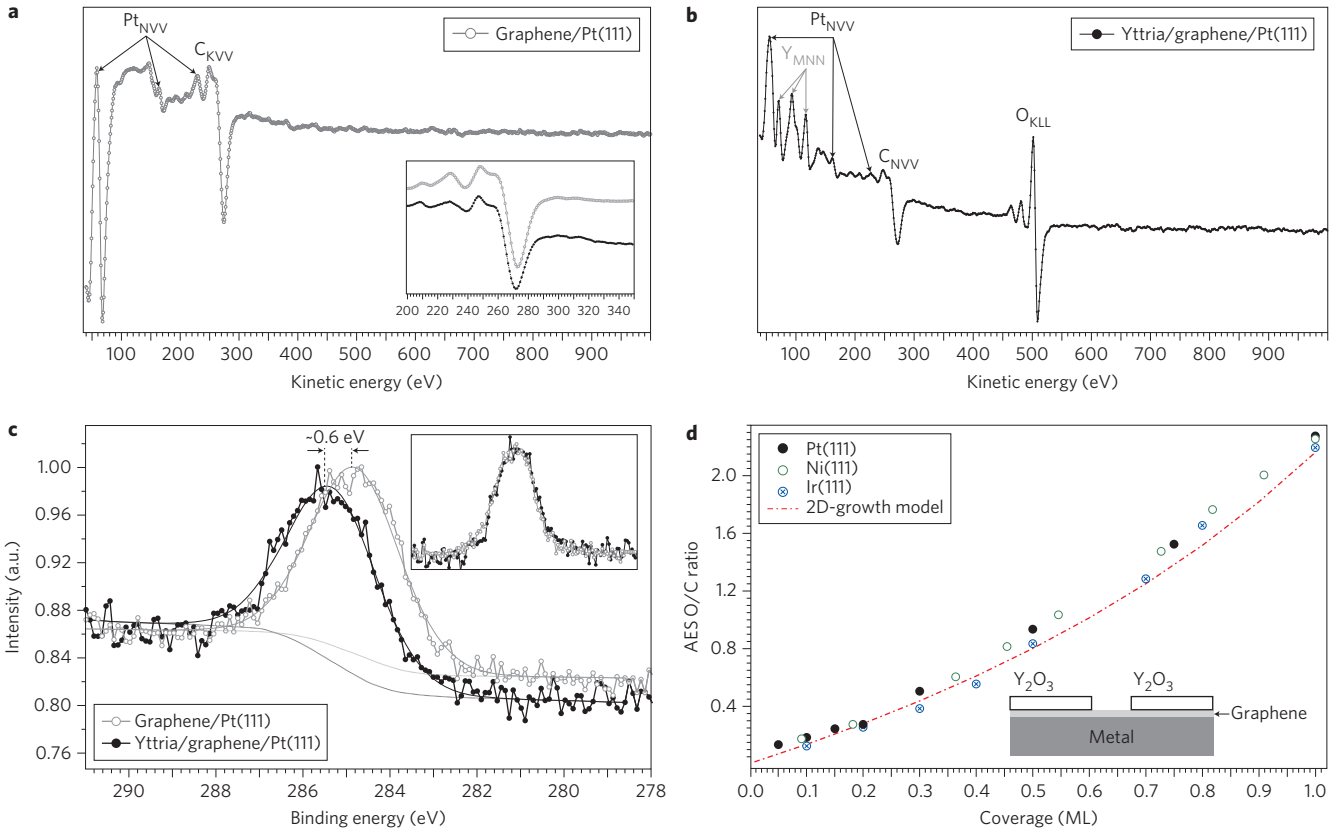

Figure 1 | AES and XPS of yttria growth on graphene/Pt(111). a,**b**, Auger survey spectra for graphene/Pt(111) (**a**) and yttria monolayer on graphene/Pt(111) (**b**). Inset (**a**): comparison of normalized C_{KVV} lines before and after yttria growth, indicating identical line shapes characteristic of sp^2 carbon. **c**, C 1s XPS spectra before and after yttria growth. The same fitting parameters are used for the C 1s peak while allowing only the peak position to vary. This indicates that the line shape remains unchanged but the peak position shifts by ~0.6 eV to higher binding energy on yttria growth. This indicates a shift of the Fermi level of graphene from ~0.3 eV below to ~0.3 eV above the Dirac point. Inset (**c**): additional comparison of the peak shape before and after yttria deposition, showing the C 1s peaks after background subtraction, normalization and shift compensation. The overlap of the two peaks further indicates that graphene remains intact after yttria growth. **d**, Auger O/C peak ratios as a function of yttria coverage (ML, monolayer) for three different metal substrates: Pt(111), Ni(111) and Ir(111). The very similar evolution of the O/C ratio for the three substrates indicates that the yttria growth behaviour is independent of the metal substrate. Furthermore, the O/C ratio follows that of a two-dimensional yttria growth model (shown as the dotted line; see Supplementary Information for a description of the model).

In the XPS measurements, Y 3*d* and O 1*s* peaks (Supplementary Fig. S5) are observed at 158.8 eV and 530.7 eV, respectively, consistent with an yttria film[27]. In Fig. 1c, the C 1*s* XPS data are presented. A rigid shift by ~0.6 eV to higher binding energy after yttria deposition on graphene/Pt(111) is observed for C 1*s*, but its line shape does not change. The peak shift to higher binding energy and also the stability of the peak shape cannot be explained by a change in the chemical state of carbon; in particular, carbide or C–O bond formation can be excluded. Accordingly, the XPS observation is consistent with the conclusions from LEED and AES that the graphene stays intact. Furthermore, the lack of a second C 1*s* component indicates the absence of any carbon–yttria bond formation. Consequently, the ~0.6 eV shift to higher binding energy is explained by a shift in the Fermi level in graphene from p-type on pure platinum[19,20] to n-type for an yttria-covered surface (see Supplementary section, 'Graphene charge doping and its determination by C 1*s* core level photoemission spectroscopy'). The shift in the Fermi level of graphene indicates that dielectric layers on metal-supported graphene can strongly affect the charge transfer from the metal to graphene, so such sandwich structures represent a potential approach for tuning the charge doping of graphene.

Figure 2 presents STM images of yttria deposited on graphene and annealed to 600 °C. The STM studies show that isolated two-dimensional yttria islands initially form, and eventually cover the entire surface with a two-dimensional yttria film. Further yttria deposition results in the formation of three-dimensional yttria clusters. The two-dimensional film may therefore be described as a wetting layer of yttria on graphene. The most characteristic feature in STM is the long-range, (pseudo) hexagonal superstructure with a small corrugation in STM of 0.33 ± 0.1 Å. The appearance of this superstructure varies only slightly across the surface, in clear contrast to the graphene/Pt(111) surface, which exhibits different periodic moiré patterns depending on the rotation angle of the graphene relative to the Pt(111) substrate[24,25]. The fact that the graphene/Pt(111) moiré structures are no longer observed indicates that the superstructure in the yttria film is not related to the Pt(111)-induced moiré pattern in graphene. Instead, it suggests that it is a consequence of lattice mismatch between graphene and the yttria film.

Inspection of the STM images in Fig. 2 reveals that although the periodicity of the superstructure does not change, several rotational domains are present in the same image. Such a rotation of the lateral superstructure without changes in its periodicity can only be explained for a simultaneous rotation of the graphene and yttria layers. In other words, the yttria layer adopts a fixed rotational relationship relative to the graphene, and the superstructure rotates with every rotational domain of graphene on Pt(111). Occasionally (Fig. 2d), defects in the superstructure are observed

© 2013 Macmillan Publishers Limited. All rights reserved.

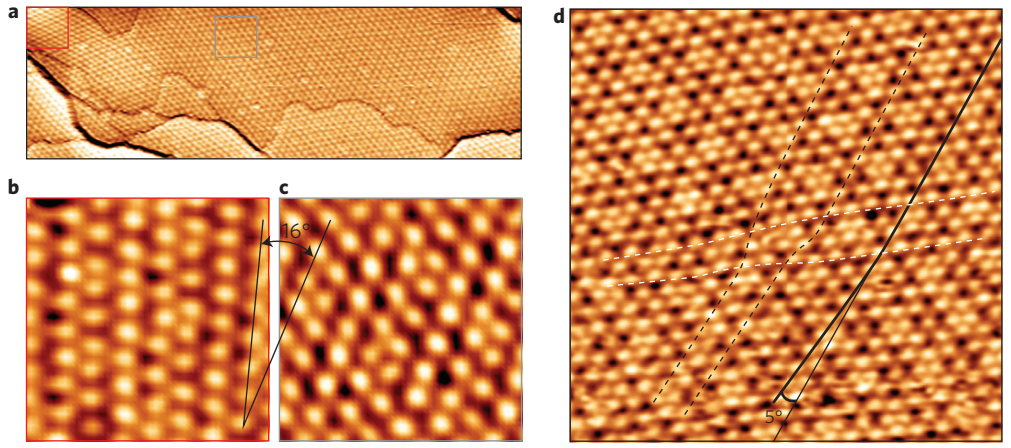

Figure 2 | STM images of yttria overlayer on graphene/Pt(111). A superstructure with a (pseudo) hexagonal order is formed. **a**, The entire surface is covered with a single-periodicity structure (dimensions of image, 165 nm × 40 nm). However, different rotational domains are observed. **b**,**c**, Enlarged images (18 nm × 18 nm) of the regions indicated in **a**. The two lattices are rotated by 16° relative to each other. **d**, Occasional twist-domain boundaries with dislocation-like cores are observed for a 5° rotation between domains. Image dimensions in **d**, 50 nm × 50 nm. STM imaging conditions: $V_{bias} = 1.0$ V, $I_t = 1.0$ nA (**a**–**c**); $V_{bias} = 0.5$ V, $I_t = 1$ nA (**d**).

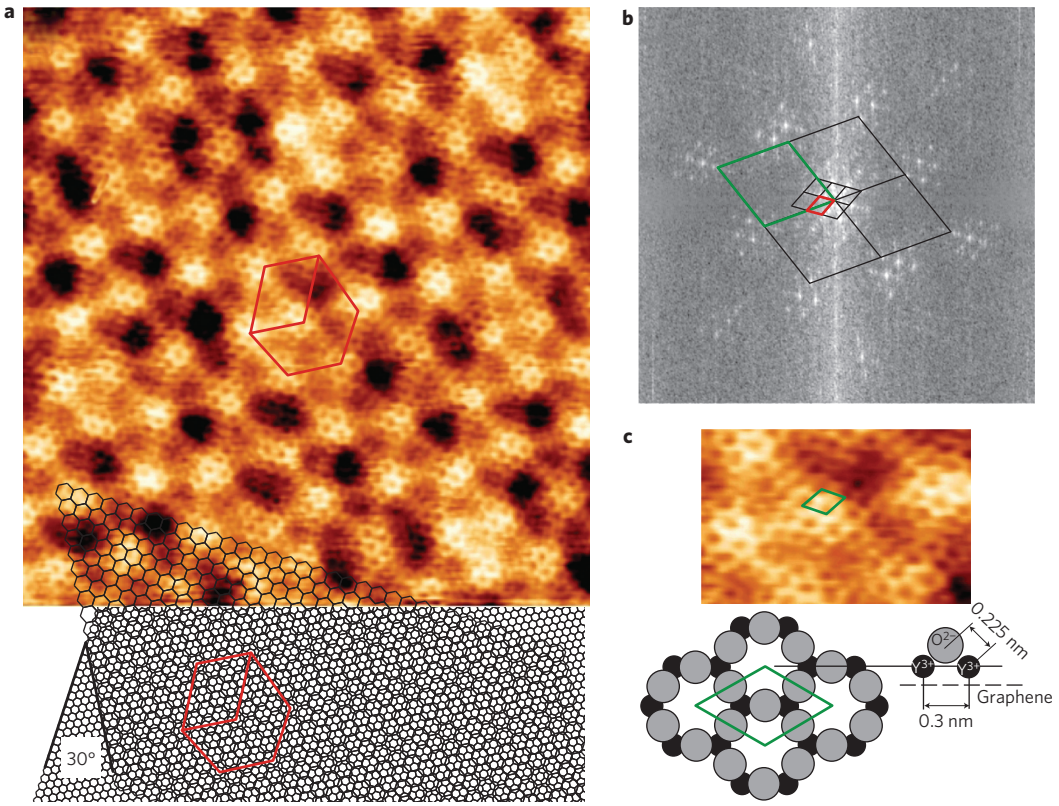

Figure 3 | High-resolution STM studies of yttria monolayer structure. a, The hexagonal yttria lattice is visible and superimposed on the long-range superstructure. The atomic honeycomb lattice of the yttria film is rotated by 30° relative to the pseudo-hexagonal superstructure. Image dimensions, 22 × 23 nm. STM imaging conditions: $V_{bias} = 8$ mV, $I_t = 2.0$ nA. **b**, The rotation is more clearly seen in the Fourier transform of the STM image. Such a rotation will occur if the yttria atomic lattice is rotated by 30° relative to the graphene honeycomb, which has unit cell dimensions about half those of the yttria. This scenario and the resulting pseudo-hexagonal superstructure is indicated at the bottom of **a**. **c**, Possible model for the yttria unit-cell structure with a Y_2O_3 composition and hexagonal symmetry, with the primitive unit cell indicated.

that are analogous to dislocation cores in small-angle tilt boundaries, thus indicating a mechanism for introducing rotation in a continuous yttria film. The fact that the yttria film maintains rotational registry with the graphene indicates a preferential alignment between this pair of two-dimensional layers. On the other hand, there is no strong interaction that would force a pseudomorphic growth of the yttria layer.

Figure 3 presents high-resolution STM images that reveal atomic-scale details of the yttria monolayer. These indicate a hexagonal lattice for the yttria film with a lattice constant that is about

© 2013 Macmillan Publishers Limited. All rights reserved.

twice that of graphene, that is, 4.9 ± 0.4 Å. Interestingly, the hexagonal unit cell of the yttria film is rotated by 30° with respect to the pseudo-hexagonal superstructure. This rotation is more clearly visible in the Fourier transform of the STM image (Fig. 3b). Such a rotation between the hexagonal yttria unit cell and the superstructure is explained if the two honeycomb atomic lattices of graphene and yttria are rotated by 30° relative to each other. This is illustrated at the bottom of Fig. 3a for two hexagonal lattices with unit-cell vectors differing by a factor of two. Such a rotation does not give a perfectly periodic superstructure; that is, no perfect hexagonal superstructure unit cell can be picked out, in agreement with our STM observations.

The formation of oxide wetting layers with structures very different from those of bulk oxides is regularly observed for oxides on metal substrates (see Supplementary Fig. S3 for yttria/Pt(111)). Wetting of graphene by an oxide, on the other hand, was unexpected. The fact that the two-dimensional yttria film forms a moiré-like superstructure on graphene allows us to reach two conclusions about its structural properties: (i) it is a contiguous film, rather than an array of individual yttrium oxide molecules, and (ii) the in-plane bonds of the two-dimensional yttria layer are stronger than interactions with the graphene substrate, so no pseudomorphic layer is formed. This therefore suggests that there exists a two-dimensional form of yttria that can be stabilized on the graphene/Pt(111) substrate. Other two-dimensional phases of bulk materials have been demonstrated or proposed previously, for example for GaN (refs 28,29), ZnO (ref. 30) or TiO_2 (ref. 31). Weak interaction between graphene and the oxide, plus the presence of the metal to balance possible dipoles in the ionic yttria film, may assist in the formation of such a novel two-dimensional yttria phase. A possible structural model for an yttria monolayer may be inspired by the previously observed structure of the isovalent V_2O_3 wetting layers on Pd(111) (ref. 32). By combining such a structural model with the lattice constant measured in our STM studies for the yttria layer and taking the typical Y–O bond length of 2.25 Å (ref. 33), a reasonable out-of-plane bond angle between yttrium and oxygen of ~45° is obtained. This structural model is displayed in Fig. 3c.

The key advance reported in this study is the formation of a two-dimensional yttria wetting layer on graphene. Graphene synthesis on metal supports, particularly copper, is one of the most promising methods for graphene wafer fabrication[22,23]. The growth of yttria on other metal-supported graphene substrates is expected to be very similar, because the chemical interaction is dominated by nearest-neighbour interactions, that is, graphene–yttria. To test this we have grown yttria films on graphene supported on Ni(111) and Ir(111) substrates and measured the evolution of the O/C AES ratios as a function of deposition time, as shown in Fig. 1d. In both cases, the evolution was identical (within experimental uncertainty) to that of yttria/graphene/Pt(111), indicating the same monolayer growth. Furthermore, detailed analysis of the evolution of the O/C peak ratios shows that this is also in excellent agreement with a simple two-dimensional growth model (see Supplementary section, 'Procedure for estimating O/C ratios in Auger measurements for a 2D oxide layer growth on graphene'). Consequently, yttria functionalization of graphene may be incorporated into the formation of large-scale graphene wafers on various metal supports. Such yttria monolayers may act as an atomic buffer or nucleation layers between graphene and other materials in subsequent processing steps.

Methods

All samples were prepared and characterized in UHV. Three different UHV chambers were used. The first chamber was equipped with an Omicron VT-STM and rear-view LEED optics. The second chamber housed a double-pass cylindrical mirror analyser with built-in electron gun for AES and front-view LEED optics. The third chamber was used for XPS measurements and was equipped with a five-channel hemispherical electron energy analyser (PSP Vacuum Technology) and a dual-anode X-ray source. All chambers were also equipped with sample preparation equipment, including sample heating, argon-ion sputter gun, precision-leak valves for oxygen and C_2H_4 dosing, and a mini electron-beam evaporation source (tectra GmbH) for yttrium vapour deposition. The Pt(111) sample was cleaned by repeated ion-sputtering annealing cycles. To clean the sample, it was annealed to 800 °C, followed by annealing in 1×10^{-7} torr O_2 at 700 °C for 10 min to burn off carbon. Graphene was grown on the clean Pt(111) sample by exposure to 1×10^{-7} torr C_2H_4 at 700 °C for 10 min. This procedure resulted in a full monolayer coverage of the Pt(111) sample with graphene. Several graphene domains with different rotational angles were observed, as reported previously. The graphene/Pt(111) surface was then used as a substrate for yttria growth. Yttrium was evaporated by electron-beam bombardment from a ~6-mm-diameter yttrium ingot supported on a molybdenum rod inside a water-cooled copper shroud. The yttrium was deposited with the sample at room temperature in a 1×10^{-7} torr O_2 atmosphere. Subsequently, the sample was annealed in vacuum to the desired target temperature. The graphene was found (by AES and XPS) to remain stable to annealing temperatures up to 750 °C; at this temperature the carbon signal decreases, possibly because of disintegration of the graphene, and carbon diffusion into the bulk. The XPS spectrometer was calibrated relative to the C 1*s* binding energy for graphene on Pt(111), which has previously been reported to be 283.9 eV. All measured peak shifts are absolute shifts of the C 1*s* peak.

Received 16 May 2012; accepted 12 November 2012; published online 23 December 2012

References

1. Robinson, J. A. *et al.* Epitaxial graphene materials integration: effects of dielectric overlayers on structural and electronic properties. *ACS Nano* **4,** 2667–2672 (2010).
2. Zhu, W. J., Neumayer, D., Perebeinos, V. & Avouris, P. Silicon nitride gate dielectrics and band gap engineering in graphene layers. *Nano Lett.* **10,** 3572–3576 (2010).
3. Farmer, D. B. *et al.* Utilization of a buffered dielectric to achieve high field-effect carrier mobility in graphene transistors. *Nano Lett.* **9,** 4474–4478 (2009).
4. Garces, N. Y. *et al.* Epitaxial graphene surface preparation for atomic layer deposition of Al_2O_3. *J. Appl. Phys.* **109,** 124304 (2011).
5. Wheeler, V. *et al.* Fluorine functionalization of epitaxial graphene for uniform deposition of thin high-kappa dielectrics. *Carbon* **50,** 2307–2314 (2012).
6. Jandhyala, S. *et al.* Atomic layer deposition of dielectrics on graphene using reversibly physisorbed ozone. *ACS Nano* **6,** 2722–2730 (2012).
7. Alaboson, J. M. P. *et al.* Seeding atomic layer deposition of high-*k* dielectrics on epitaxial graphene with organic self-assembled monolayers. *ACS Nano* **5,** 5223–5232 (2011).
8. Fallahazad, B. *et al.* Scaling of Al_2O_3 dielectric for graphene field-effect transistors *Appl. Phys. Lett.* **100,** 093112 (2012).
9. Han, W. *et al.* Spin transport and relaxation in graphene *J. Magn. Magn. Mater.* **324,** 369–381 (2012).
10. Lui, C. H., Liu, L., Mak, K. F., Flynn, G. W. & Heinz, T. F. Ultraflat graphene. *Nature* **462,** 339–341 (2009).
11. Dean, C. R. *et al.* Boron nitride substrates for high-quality graphene electronics. *Nature Nanotech.* **5,** 722–726 (2010).
12. Xue, J. M. *et al.* Scanning tunnelling microscopy and spectroscopy of ultra-flat graphene on hexagonal boron nitride. *Nature Mater.* **10,** 282–285 (2011).
13. Decker, R. *et al.* Local electronic properties of graphene on a BN substrate via scanning tunneling microscopy. *Nano Lett.* **11,** 2291–2295 (2011).
14. Novoselov, K. S. *et al.* Two-dimensional atomic crystals *Proc. Natl Acad. Sci. USA* **102,** 10451–10453 (2005).
15. Radisavljevic, B., Radenovic, A., Brivio, J., Giacometti, V. & Kis A. Single-layer MoS_2 transistors. *Nature Nanotech.* **6,** 147–150 (2011).
16. Xu, H. *et al.* Quantum capacitance limited vertical scaling of graphene field-effect transistor. *ACS Nano* **5,** 2340–2347 (2011).
17. Xu, H. *et al.* Top-gated graphene field-effect transistors with high normalized transconductance and designable Dirac point voltage. *ACS Nano* **5,** 5031–5037 (2011).
18. Batzill, M. The surface science of graphene: metal interfaces, CVD synthesis, nanoribbons, chemical modifications, and defects. *Surf. Sci. Rep.* **67,** 83–115 (2012).
19. Sutter, P., Sadowski, J. T. & Sutter E. Graphene on Pt(111): growth and substrate interaction. *Phys. Rev. B* **80,** 245411 (2009).
20. Giovannetti, G. Doping graphene with metal contacts. *Phys. Rev. Lett.* **101,** 026803 (2008).
21. Politano, A., Marino, A. R., Formoso, V.& Chiarello, G. Evidence of Kohn anomalies in quasi-freestanding graphene on Pt(111). *Carbon* **50,** 734–736 (2011).
22. Li, X. S. *et al.* Large-area synthesis of high-quality and uniform graphene films on copper foils. *Science* **324,** 1312–1314 (2009).
23. Bae, S. *et al.* Roll-to-roll production of 30-inch graphene films for transparent electrodes. *Nature Nanotech.* **5,** 574–578 (2010).

© 2013 Macmillan Publishers Limited. All rights reserved.

24. Merino, P., Svec, M., Pinnardi, A. L., Otero, G. & Martin-Gago, J. A. Strain-driven moire superstructures of epitaxial graphene on transition metal surfaces. *ACS Nano* **5,** 5627–5634 (2011).
25. Gao, M. *et al.* Epitaxial growth and structural property of graphene on Pt(111). *Appl. Phys. Lett.* **98,** 033101 (2011).
26. Rey, S. & Le Normand, F. Surface transformations of carbon (graphene, graphite, diamond, carbide), deposited on polycrystalline nickel by hot filaments chemical vapour deposition. *Thin Solid Films* **519,** 4426–4428 (2011).
27. Tao, J. & Batzill, M. Ultrathin Y_2O_3(111) films on Pt(111) substrates. *Surf. Sci.* **605,** 1826–1833 (2011).
28. Freeman, C. L., Claeyssens, F., Allan, N. L. & Harding, J. H. Graphitic nanofilms as precursors to wurtzite films: theory. *Phys. Rev. Lett.* **96,** 066102 (2006).
29. Chen, Q., Hu, H., Chen, X. & Wang J. Tailoring band gap in GaN sheet by chemical modification and electric field: *ab initio* calculations. *Appl. Phys. Lett.* **98,** 053102 (2011).
30. Tusche, C., Meyerheim, H. L. & Kirschner J. Observation of depolarized ZnO(0001) monolayers: formation of unreconstructed planar sheets. *Phys. Rev. Lett.* **99,** 026102 (2007).
31. Orzali, T., Casarin, M., Granozzi, G., Sambi, M. & Vittadini, A. Bottom-up assembly of single-domain titania nanosheets on (1×2)-Pt(110). *Phys. Rev. Lett.* **97,** 156101 (2006).
32. Surnev, S. *et al.* Growth and structure of ultrathin vanadium oxide layers on Pd(111). *Phys. Rev. B* **61,** 13945 (2000).
33. Belonoshko, A. B., Gutierrez, G., Ahuja, R. & Johansson, B. Molecular dynamics simulation of the structure of yttria Y_2O_3 phases using pairwise interactions. *Phys. Rev. B* **64,** 184103 (2001).

Acknowledgements

The authors acknowledge financial support from the Office of Naval Research (N00014-10-1-0668 and N00014-11-1-0779) and the National Science Foundation (DMR-1204924).

Author contributions

R.A. performed STM and XPS experiments, analysed the data, and prepared figures. A.D. performed and analysed Auger measurements. M.B. conceived the experiment and wrote the manuscript.

Additional information

Supplementary information is available in the online version of the paper. Reprints and permission information is available online at http://www.nature.com/reprints. Correspondence and requests for materials should be addressed to M.B.

Competing financial interests

The authors declare no competing financial interests.

© 2013 Macmillan Publishers Limited. All rights reserved.